LAWRENCE
LIVERMORE
NATIONAL
LABORATORY

UCRL-JRNL-205310

# An Investigation of Solid-State Amidization and Imidization Reactions In Vapor Deposited Poly(amic acid)

*Mitchell Anthamatten, Stephan A. Letts, Katherine Day, Robert C. Cook, Anthony P. Gies, Tracy P. Hamilton, William K. Nonidez*

**07/07/2004**

Journal of Polymer Science: Part A Polymer Chemistry

# DISCLAIMER

# An Investigation of Solid-State Amidization and Imidization Reactions in Vapor Deposited Poly(amic acid)

Mitchell Anthamatten*, Stephan A. Letts, Katherine Day, Robert C. Cook

Lawrence Livermore National Laboratory,

P.O. Box 808, M.S. L-474

Livermore, CA 94550 USA

Anthony P. Gies, Tracy P. Hamilton, William K. Nonidez

Department of Chemistry

University of Alabama at Birmingham,

901 14th Street South

Birmingham, AL 35294 USA

* Current Address: University of Rochester, Department of Chemical Engineering, 206 Gavett Hall, Rochester, NY, 14627.

**Synopsis**

The condensation polymerization reaction of 4,4'-oxydianiline (ODA) with pyromellitic dianhydride (PMDA) to form poly(amic acid) and the subsequent imidization reaction to form polyimide were investigated for films prepared using vapor deposition polymerization techniques. Fourier-transform infrared spectroscopy (FT-IR), thermal analysis, and matrix-assisted laser desorption/ionization time-of-flight mass spectrometry (MALDI-TOF MS) of films at different temperatures indicate that additional solid-state polymerization occurs prior to imidization reactions. Experiments reveal that, upon vapor deposition, poly(amic acid) oligomers form that have a number-average molecular weight of about 1500 Daltons. Between 100 – 130 ºC these chains undergo additional condensation reaction to form slightly higher molecular weight oligomers. Calorimetry measurements show that this reaction is exothermic ($\Delta H \sim -30$ J/g) with an activation energy of about 120 kJ/mol. Experimental reaction enthalpies are compared to results from *ab initio* molecular modeling calculations to estimate the number of amide groups formed. At higher temperatures (150 – 300 °C) imidization of amide linkages occurs as an endothermic reaction ($\Delta H \sim +120$ J/g) with an activation energy of about 130 kJ/mol. Solid-state kinetics were found to depend on reaction conversion as well as the processing conditions used to deposit films.

KEYWORDS: solid-state polymerization, polyimides, curing of polymers, coatings, activation energy, calorimetry, infrared spectroscopy

## Introduction

Polyimides are well known for their high temperature stability, low dielectric constants, good mechanical properties, and inertness to solvents. Since polyimides first became commercially available in the 1960's, they have found numerous applications ranging from aerospace to electronics to packaging.[1] In the majority of these applications, polyimides are either melt-processed to control the material's three-dimensional shape, or solution-processed to form films or coatings. A third polyimide processing option is vapor-deposition polymerization (VDP).[2] This technique, first applied to polyimides independently by Salem *et al.*[3] and Iijima *et al*.[4], is a solventless procedure that involves the coevapration of a diamine and dianhydride onto a substrate. Upon vapor-deposition, monomers undergo a solid-state condensation reaction to form a poly(amic acid) precursor, which can be converted to polyimide through a curing step at elevated temperature shown in Figure 1. VDP enables uniform coatings to be formed where the presence of a solvent is unacceptable, or where coatings are required to conform well to non-planar substrates. Vapor-deposited polyimide films are being investigated for their use as gas barriers,[5-7] conformal dielectric coatings [8-10], and inertial confinement fusion laser targets[11-16].

Despite the demand for a dry process to conformally coat polyimide, several obstacles have prevented the widespread use of this technology. Monomers are only suitable for vapor deposition if they exhibit high enough vapor pressure. The VDP process is slow—a typical film growth rate is on the order of microns per hour. VDP is expensive since it requires the use of vacuum chambers operating at ~$10^{-7}$ Torr. Lastly, many properties of vapor-deposited polyimide are markedly inferior to their solution-cast analogs. To

understand the differences between solution-processed and vapor-deposited materials, researchers have investigated how VDP processing conditions affect polyimide's strength[14,17,18], permeability [14,19], thermal stability[20], and electrical properties[21]. As one would expect, many of these properties depend strongly on molecular weight. FT-IR studies indicate that the vapor-deposited material consists of a mixture of reacted and unreacted monomers[3,22]. Dimitrikopoulos et al.[23] studied the kinetics of the solid-state reaction between PMDA with ODA in vapor-deposited films between -50 and 23 °C using FT-IR techniques. Their results indicate that reaction is limited by diffusion of monomers through the bulk of the film. They concluded that the reaction product up to room temperature consist mainly of dimers. Unfortunately, there is no straightforward way to characterize the molecular weight of polyimides because most polyimides are insoluble in organic solvents. Molecular weights of solution processed polyimides are traditionally inferred from the characterization of their poly(amic acid) precursors.[24-27] Gies and coworkers have recently developed a MALDI-TOF mass spectrometric technique for determining the solid-state molecular weight distribution of vapor-deposited poly(amic acid) and polyimide.[28] Results of their analysis confirm that the vapor-deposited material consists of oligomeric species, mostly dimers and trimers. Cured polyimide was found to be higher in molecular weight than the as-deposited poly(amic acid) suggesting that additional chain growth occurred during the curing process.

A better understanding of the solid-state amidization and subsequent imidization reactions could yield valuable insight toward optimizing the properties of vapor-deposited polyimides. This paper addresses the issues of solid-state polymerization and imidization of vapor-deposited poly(amic acid) through *in situ* FT-IR experiments, thermal analysis, and

MALDI-TOF mass spectrometry. Each technique was used to study the material at various temperatures during the curing process to determine when and to what extent chain growth reaction and imidization occurs. Through our analysis, we also examine the role that unreacted, excess monomer plays in the chain growth and imidization reactions.

## Experimental Section

**Sample Preparation.** Chemical vapor deposition of ODA and PMDA was carried out to yield films of poly(amic acid). Equivalent amounts of PMDA and ODA (~ 10 g) were loaded into separate Knudsen cell evaporators. These evaporators were positioned inside a vacuum chamber, 70 mm above the target substrate. Heating cartridges were embedded into each evaporator to supply power, and thermocouples were used to monitor the temperatures. To deposit films, evaporators were heated to controlled temperatures under vacuum conditions (~$10^{-7}$ Torr), and a shutter covering the substrate was moved aside. Deposition rates were measured to be about 25 μm / hour. During deposition, due mainly to radiant heating from the evaporators, the substrate temperature was measured to be 62 °C. Further experimental details relevant to this process have been published elsewhere.[29]

In discussing the dose conditions it is convenient to define the monomer flux ratio as $\rho = N_{PMDA} / N_{ODA}$ where $N_i$ is the molar flux of monomer leaving the evaporators. An equal molar flux ($\rho = 1.0$) is achieved if evaporator temperatures are controlled to 192 ± 0.2 °C for PMDA and 176 ± 0.2 °C for ODA. Note that $\rho$ only defines the vapor composition leaving the evaporators and does not define the composition of the as-deposited film. We found that PMDA preferentially reemits from the target substrate. During deposition a white powder

was observed to condense onto the glass of the vacuum chamber. This material was analyzed using FT-IR and the resulting spectrum agrees with that of pure PMDA. Thus, for $\rho = 1$ the as-deposited poly(amic acid) is lean in PMDA and rich in unreacted ODA.

**FT-IR Spectroscopy.** A Perkin-Elmer FT-IR spectrometer (model: Spectrum 2000) was used to characterize samples that were solution-cast or vapor-deposited onto 13 x 1 mm KBr optics. Data were collected as the percent-transmission $T(\lambda)$ over the IR spectrum (500 - 7800 $cm^{-1}$) at a resolution of 4 $cm^{-1}$. A background spectrum taken of an uncoated KBr optic was automatically subtracted from each scan. Following this baseline correction, data were converted to absorbance defined by $A(\lambda) = -\ln T(\lambda)$. The measured absorbance then consists of 1) excitation of vibrational modes, 2) reflection from material surfaces, and 3) internal material scattering due to electron density fluctuations.

For *in situ* curing experiments, samples were coated onto KBr optics and were sandwiched between apertured aluminum disks in a custom-machined sample holder designed to ensure good thermal contact. An external temperature controller (ColeParmer) was used to monitor the temperature and control the supply of power sent to the sample holder. Using this method, temperature control was achieved to ± 1 °C. Curing runs were conducted at a heating rate of 2 °C/min. During curing, the sample chamber was purged with nitrogen to protect the IR detector and to avoid hydrolysis of the poly(amic acid).

**Thermal Analysis.** Differential scanning calorimetry (DSC) and thermal gravimetric analysis (TGA) were performed on several vapor-deposited samples. TGA experiments were executed using a Perkin-Elmer Pyris 1 TGA scanning from 50 to 700 °C at rates of 2, 5, 10, 20, and 40 °C/min. For DSC analysis, small amounts (~15 mg) of poly(amic acid) were loaded into aluminum pans. DSC scans were performed using a Perkin-Elmer Diamond

DSC, scanning from 25 to 400 °C at rates of 5, 10, 20, 40, and 100°C/min. Heating and cooling cycles were repeated to test for reversibility.

**MALDI-TOF MS Measurements.** Samples were analyzed using a Voyager Elite MALDI-TOF MS system (Perkin-Elmer PerSeptive Biosystems) operating with a 337-nm $N_2$ laser. Spectra were obtained in positive-ion mode with an accelerating voltage of 20 kV and a laser intensity ~ 10% greater than threshold. Mass calibration was performed before and after each experiment by running Angiotension I (1296.69 g/mol) and Insulin B (3496.96 g/mol) from a Sequazyme Peptide Mass Standard Kit. Prior to analysis poly(amic acid) samples were heated to various temperatures using a Frontier Labs double-shot pyrolyzer equipped with platinum sample holders. Samples were then prepared by the evaporation-grinding method[28,30] using 3-aminoquinoline (3AQ, Aldrich) as a matrix, potassium trifluoroacetate (KTFA, Aldrich) as a dopant, and THF as a solvent. Samples were run using a molar ratio of 25:1:1 (3AQ : poly(amic acid) : KTFA).

## Results and Discussion

**FT-IR spectra of vapor-deposited ODA/PMDA during cure.** Figure 2 shows FT-IR absorption spectra of as-deposited poly(amic acid) from 1900 $cm^{-1}$ to 1200 $cm^{-1}$ at selected temperatures during a curing run. Vibrational modes corresponding to relevant peaks are listed in Table 1 and are based on peak assignments made by others.[3,23] The room temperature FT-IR spectrum of as-deposited poly(amic acid) will be briefly discussed. The FT-IR absorption at 1664 $cm^{-1}$ is assigned to the amide carbonyl stretch. This peak confirms the formation of poly(amic acid) condensation products. The amide linkage is also indicated

by absorption at 1543 $cm^{-1}$ arising from the N-H bending mode, and 1324 $cm^{-1}$ due to C-N stretching. The peaks at 1852 and 1780 $cm^{-1}$ are from anhydride moieties and suggest that unreacted anhydride groups are present, either as unreacted monomer or as end-groups on the oligomer chains. The carboxylic acid group in poly(amic acid) is indicated by a broad O-H stretch signal at 3400 $cm^{-1}$ (not shown in the figure). Free carboxylic acid groups can be deprotonated by the weak amine base. Consequently, carboxylate ions (COO-) are also present and exhibit stretching at 1606 and 1415 $cm^{-1}$.

To quantitatively account for the chemical changes occurring during cure, peak analysis was performed. To do this, FT-IR absorbance data were assumed to consist of the sum of a background contribution and several Gaussian curves—each curve corresponding a different vibrational mode. The background contribution was taken as the absorbance at 1900 $cm^{-1}$. This location was chosen because it is near the wavelengths of interest (1200 to 1900 $cm^{-1}$) yet there appear to be no contribution from vibrational modes. The integrated peak intensity $I_\upsilon$ of a Gaussian distribution centered at a frequency $\upsilon$ is proportional to the sample concentration of functional groups vibrating at $\upsilon$. Deconvolution of neighboring peaks was achieved by fitting the center position, width, and maximum intensity of each Gaussian using a non-linear regression routine.[31] The inset in Figure 2 illustrates the peak analysis process by comparing raw absorbance data to a curve obtained from a sum of Gaussians. This approach is necessary because the peak intensity can be affected by neighboring shoulder peaks, and peak-broadening effects may arise due to subtle differences between end-segment and center-segment vibrations.

Figure 3 summarizes the results of the peak analysis. Integrated peak intensities, normalized by their maximum value, are plotted against temperature from 25 to 300 °C. This

enables all data to be plotted against the same ordinate. Data indicate that the concentration of amide linkages, corresponding to the carbonyl peak centered at 1664 $cm^{-1}$ and the N-H bending mode at 1543 $cm^{-1}$ (not shown) first increases between 100 and 130 °C before decreasing upon imidization. The growth in the amide signal combined with the concomitant decrease in the integrated peak intensity of anhydride vibrations at 1852 $cm^{-1}$ and 1780 $cm^{-1}$ (not shown) confirm that solid-state amidization reaction is occurring. At higher temperatures, strong FT-IR peaks develop at the frequencies expected for the imide functionality, namely 1380 and 1728 $cm^{-1}$ (not shown). The fraction $I_{1380}/ I_{1380, max}$ can be used to monitor fractional conversion of solid-state imidization. Also, during imidization the anhydride peaks at 1852 and 1780 $cm^{-1}$ almost completely disappear. This suggests that some anhydride groups that were not consumed in the chain-growth reactions are hydrolyzed during imidization. Hydrolysis is facilitated by the presence of water that is generated as a by-product of the imidization reaction.

**Thermal analysis of vapor-deposited ODA/PMDA.** Thermal analysis is well suited to study kinetics because of superior temperature control, though it foregoes information regarding chemical changes. In this section thermal analytical techniques will be used to investigate the kinetics of two solid-state reactions: the imidization curing reaction and the amide chain-growth reaction occurring at lower temperatures.

To investigate how the presence of excess monomer affects the solid-state reactions, samples were vapor-deposited under different coating conditions, i.e. using different values of the monomer flux ratio $\rho$. A summary of the poly(amic acid) coatings deposited for thermal analysis is included in Table 2, and examples of thermogravimetric curves acquired at 2 °C /min for each of the five samples are shown in Fig. 4. Three thermal transitions are

evident from the TGA data: imidization, sublimation of excess ODA, and thermal decomposition. Since VDP is a solventless process, solvent removal prior to characterization is not an issue and data are not be convoluted by solvent decomplexation[18,32,33].

The first mass loss in Figure 4 occurs at about 150 °C and is due to the loss of water molecules as amide linkages are converted into imide linkages. Following this transition, data are nearly level around 230 °C. This initial mass loss of about 7-8% mass loss agrees well with the theoretical mass loss of 8.6 % in the limit where poly(amic acid) chains are of infinite length. Solid-state imidization reaction kinetics were studied by repeating TGA runs at several different heating rates as illustrated in Figure 5 for ρ = 1.16. From these curves, the conversion or extent of imidization $\alpha_{im}$ can calculated at any temperature directly from the TGA curves as

$$\alpha_{im}(T) = \frac{(1-m)}{(1-m_{im})} \qquad [1]$$

where $m$ is the mass fraction remaining during a TGA run and $m_{im}$ is the final mass fraction remaining following imidization. The value of $m_{im}$ (at full conversion) was estimated by the intersection of lines drawn tangent to the TGA data prior and after the end of this transition see dashed lines in Figure 4). As expected, greater conversions are observed at lower temperatures in experiments conducted at slower heating rates. The heating rate was found to have little influence on the ultimate degree of imidization.

The activation energy of the solid-state imidization reaction was estimated using the Kissinger method.[34-36] The Kissinger method is an isoconversion (constant heating rate)

method that has been applied to a broad range of solid-state reactions and it involves no prior assumption of the reaction order. The result of Kissinger is that

$$\ln\left(\frac{\beta}{T_f^2}\right) = -\frac{E_a}{RT_f} + C_2 \qquad [2]$$

where $\beta$ is the heating rate, $T_f$ is the temperature at a given fractional conversion, $E_a$ is the activation energy, $R$ is the gas constant, and $C_2$ is a parameter independent of $T$ and $\beta$. According to eqn. 2, plots of $\ln(T_f^2/\beta)$ versus $1/T_f$ should yield straight lines with a slope of $E_a/R$. Figure 6 shows a typical Kissinger plot for a poly(amic acid) sample obtained from TGA runs at five different heating rates. The data are nearly linear and activation energies were calculated for all levels of conversion ($\alpha_{im}$) shown in Figure 6 for $\rho = 1.16$. This analysis was repeated for each sample. The resulting activation energies range from 114 to 178 kJ/mol and are plotted against the imidization conversion in Figure 7. All samples exhibit higher activation energies as the reaction nears completion. This is not surprising since in the solid-state there should exist a distribution of activation energy barriers that depend on local chemical environments, chain mobility, and packing considerations. Interestingly, the sample deposited with the largest excess PMDA ($\rho = 1.31$) exhibits the highest activation energies. One could argue that this sample's actual film composition is closer to a stoichiometric ratio of 1:1 (in PMDA:ODA), and consequently longer chains can form which, in turn, have lower mobility. For all other samples, $\rho$ does not appear to be correlated with $E_a$.

The second stage of mass loss, denoted in Figure 4 as $m_{ODA}$, occurs mainly between 300 and 400 °C and is attributed to sublimation of unreacted ODA monomer. This was determined by placing a cold glass cover slip over samples that were heated to 350 °C. After several minutes a white powder condensed on the cover slip. This material was analyzed using FT-IR and identified to be ODA. Furthermore, the fractional mass loss due to reemission of ODA is consistent with the monomer flux ratio used during deposition. Samples deposited with a high monomer flux ratio (more PMDA) showed much less ODA reemission and vice versa for samples with a lower monomer flux ratio (for $\rho$=1.31 $m_{ODA}$ =0.09 where for $\rho$=0.68 $m_{ODA}$=0.16).

The thermogravimetric curves in Figure 4 show additional mass loss between 450 and 550 °C. In this region, the rate of mass loss appears to be independent of $\rho$, and thus is not related to excess monomer. At these temperatures samples begin to darken suggesting that thermal degradation is occurring. Above 600 °C the material is clearly undergoing thermal degradation as evidenced by rapid mass loss and darkening of the films.

Table 3 summarizes the mass losses associated with imidization and sublimation of ODA obtained from the TGA experiments. If one assumes that, during imidization, all amide linkages were converted to imide linkages, then, the mass change due to water loss can be related to the average degree of polymerization of the polyimide chains. By ratioing the measured water loss to the theoretical water loss of 8.6% for infinite chains the extent of reaction for the amidization reaction $\alpha_{am}$ can be calculated (not to be confused with $\alpha_{im}$). The average degree of polymerization $x$ is then obtained from the well-known Carothers' equation: $x = 1 / (1- \alpha_{am})$. Bearing in mind that $x$ becomes increasingly sensitive to $\alpha_{im}$ as $\alpha_{im}$

approaches unity, the results in Table 3 suggest that the calculated degree of polymerization is lowest for samples with more ODA.

DSC analysis was used to study the solid-state kinetics of the condensation polymerization (amidization) reaction. Figure 8 shows DSC heating scans of a typical vapor-deposited poly(amic acid) sample (PAA98) acquired at several different heating rates. Depending on the heating rate, samples exhibit an exothermic peak between 110 and 160 ºC followed by an endothermic peak between 160 and 280 ºC. The FT-IR spectra discussed in Section 3.1 suggest that the exothermic transition is due to chain-growth (amidization), and the endothermic peak is due to imidization. Unfortunately, in the DSC analysis these two thermal transitions partially overlap—this is especially true for data acquired at fast heating rates. To avoid this issue, and to examine the kinetics of the solid-state chain growth reaction, we apply the following approximation to the exothermic peak: the maximum rate of transformation occurs at a fixed extent of reaction $\alpha_{am}$. This assumption carries with it a small error[36], but it enables one to apply the Kissinger method where $T_f$ is taken as the temperature corresponding to the peak of the exotherm in the DSC scans. Figure 9 shows plots of $\ln(T_f/\beta)$ with linear fits versus $1/T_f$ for different values of $\rho$. The data appear fairly linear although they begin to deviate from linearity at lower scanning rates (higher values of $1/T_f$). Based on the slopes of linear fits to the data in Figure 9, the activation energy for the amidization reaction is estimated to be 120 ± 10 kJ/mol.

Reaction enthalpies and activation energies obtained from DSC and TGA experiments are summarized in Table 4. Values for reaction enthalpies were determined from DSC data acquired at 40 °C/min—similar values were obtained at other heating rates. Note that the measured enthalpy changes of the amidization reaction (chain growth) only

correspond to *additional* condensation that occurs upon heating. Many amide groups had already formed upon film deposition, prior to the heating scan. Indeed, the data in Figure 3 suggest that over one half of amide groups were present, prior to any thermal treatment. On the other hand, the measured enthalpy changes due to imidization correspond to the conversion of all amide linkages to imide rings. Slightly greater enthalpy changes (per gram) are observed for both the amidization and imidization reactions at higher monomer flux ratios. These results are consistent with the picture that at high monomer flux ratios the as-deposited material is closer to 1:1 stoichiometry (PMDA:ODA). At stoichiometric equivalence more condensation reactions can occur, that is, longer polymer chains can form—as such, one would expect these samples to exhibit higher activation energies. Indeed, activation energies for both reactions are greatest for samples deposited at the highest monomer flux ratios ($\rho = 1.31$).

**MALDI-TOF MS Analysis.** Mass spectra from MALDI-TOF MS measurements at selected temperatures are shown in Figure 10. All mass spectra show molecular weight distributions that are dominated by short oligomeric chains as shown in our earlier investigation.[28] Green peaks indicate masses that are consistent with poly(amic acid) chains, blue peaks indicate partially imidized chains, and red peaks indicate polyimide chains. After thermal treatment at 130 ºC a mixture of all three species are present, and after treatment at 300 ºC only imidized chains are present. Both the number-average and weight-average molecular weight increased following thermal treatment; this confirms solid-state chain growth reactions have occurred. A more detailed MALDI-TOF MS study that focuses on the thermal behavior of these materials has been published elsewhere[37].

**Calculation of B3LYP/6-31G(d) and MP2 (fc)/6-311G(2d,p)//B3LYP/6-31G(d) reaction energies.** The reaction enthalpies provided in Table 4 are of limited use because they are on a per-mass basis. Alone, these values imply little about the degree of conversion for either the amidization or imidization reactions. In order to address this issue and to evaluate the consistency of the FT-IR, TGA/DSC, and MALDI-TOF MS experiments, we have applied computational techniques to estimate molar reaction enthalpy and entropy changes. Naturally, in the solid-state, non-covalent intermolecular interactions will play important roles in determining a molecule's energy state. All such interactions are neglected in the series of simple "gas-phase" calculations presented here. Our goal is not to accurately predict thermodynamic quantities in the solid-state but rather to confirm our understanding of the relative energy levels of molecular species.

A Monte Carlo conformational search was performed on the dimer of the anhydride and the amine at the AM1 level of theory, using SPARTAN 02 for Windows.[38] Four isomers were found which differed in their pattern of intramolecular hydrogen bonding. The most stable structure had an H-bond from the amide N-H to the carbonyl of the acid group. Each of these structures was then optimized at the B3LYP/6-31G(d) level of theory using Gaussian98.[39] There were some slight changes in relative energies, but the isomer with the H-bond between the amide N-H and the acid carbonyl remains the global minimum.

The structures were all confirmed to be minima by computation of the vibrational frequencies. The vibrational frequencies also enable the computation of enthalpy and entropy. The temperature selected as being most appropriate for comparison to the experiments was 130 °C. The enthalpy of reaction was computed by H(product)-H(reactants) to be -44.4 kJ/mol. Since B3LYP/6-31G(d) performs much better for predicting

geometries than relative energies, single point MP2 (fc)/6-311G(2d,p)//B3LYP/6-31G(d) energies were computed. Using the thermal corrections from B3LYP with the MP2 energies, the reaction enthalpy is predicted to be a bit more exothermic at -69.9 kJ/mol. Based on the MP2 energies, we estimate the reaction enthalpy corresponding to full conversion (formation of an infinite chain) at 130 °C of a 1:1 mixture of the diamine and the dianhydride is about -320 J/g. This value is about a factor of ten higher than the enthalpy we measured using DSC and suggests that conversion increases by a small amount (~10%) during cure. This idea is consistent with the FT-IR experiments which show the presence of amide groups upon deposition, and a small increase in the concentration of amide groups during cure. Likewise, the MALDI-TOF MS results also indicate a modest increase in molecular weight (about 10%) that occurs upon curing.

The formation of the imide by condensation was also studied at the B3LYP/6-31G(d) and MP2(fc)/6-311G(2d,p)// B3LYP/6-31G(d) levels of theory. This step is predicted by theory to be slightly endothermic. The enthalpy change for imide formation at 130 C is +29.9 and +8.4 kJ/mol for B3LYP and MP2, respectively. These results predict that the conversion of a poly(amic acid) infinite chain to a polyimide infinite chain would require about +140 J/g and +40 J/g for B3LYP and MP2, respectively. The experimentally determined imidization enthalpies (Table 4) are about +120-160 J/g which agree well with the B3LYP method but are in disagreement with the MP2 method by a factor of three to four. This discrepancy becomes even larger if one considers the MALDI-TOF MS experimental results that suggest the polymer chains are short and there are fewer imide linkage groups present per unit mass.

## Concluding Remarks

FT-IR, thermal analysis, and MALDI-TOF mass spectrometry have been used to study the solid-state condensation polymerization reaction of ODA with PMDA in vapor deposited films. We have confirmed that between 100-130 ºC additional solid-state chain growth condensation reactions occur. Experiments coupled with molecular modeling results suggest that the solid-state chain growth is modest (~10%) and does not lead to high molecular weight poly(amic acid). The solid state activation energy for this process was measured to be 110-130 kJ/mol. As expected, experiments confirmed that at higher temperatures (150-250 °C) the imidization reaction is endothermic ($\Delta H \sim +120$ J/g), and, interestingly, the activation energy for this process (110-180 kJ/mol) increases with the degree of imidization. This result is consistent with a distribution of activation energies due to differences in local molecular environments. Finally, for both amidization and imidization reactions, samples with higher monomer loss ratios (PMDA:ODA) showed larger reaction enthalpy changes per unit mass. This result suggests that a monomer loss ratio greater than one may be required to form films close to 1:1 stoichiometry.

## Acknowledgements

This work was performed under the auspices of the U. S. Department of Energy by the UC, Lawrence Livermore National Laboratory under Contract W-7405-ENG-48.

**Table 1**. FT-IR assignments for vapor deposited poly(amic acid) and polyimide.

| no. | frequency ($cm^{-1}$) | vibrational mode |
|---|---|---|
| 1 | 1852 | anhydride ring symmetric anhydride ring stretch |
| 2 | 1780 | anhydride ring asymmetric carbonyl stretching |
| 3 | 1728 | imide carbonyl stretching |
| 4 | 1715 | amic acid carbonyl stretching |
| 5 | 1664 | amide carbonyl stretching |
| 6 | 1627 | ODA aromatic ring mode |
| 7 | 1606 | asymmetric stretch of carboxylate ion ($COO^-$) |
| 8 | 1543 | amide N-H bending mode |
| 9 | 1503 | ODA aromatic ring mode |
| 10 | 1415 | symmetric stretch of carboxylate ion ($COO^-$) |
| 11 | 1380 | imide peak |
| 12 | 1324 | amide C-N stretching mode |
| 13 | 1241 | ether C-O-C and anhydride C-O-C stretching |

**Table 2.** Vapor-deposited poly(amic acid) samples characterized using thermal analysis.

| sample | $T_{ODA}$ (°C) | $T_{PMDA}$(°C) | $\rho = N_{PMDA}/N_{ODA}$ | measured coating rate (μm/hour) |
|---|---|---|---|---|
| PAA68 | 180 | 192 | 0.68 | 52.8 |
| PAA75 | 167 | 174 | 0.75 | 28.6 |
| PAA98 | 176 | 192 | 0.98 | 39.0 |
| PAA116 | 165 | 174 | 1.16 | 23.1 |
| PAA131 | 172 | 192 | 1.31 | 28.3 |

**Table 3.** Summary of TGA experiments

| monomer loss ratio | % mass loss from imidization[a] | % mass loss from ODA sublimation[a] | calculated extent of reaction, $\alpha_p$ | calculated average degree of polymerization |
|---|---|---|---|---|
| 0.68 | 6.9 | 11.8 | 0.80 | 5.1 |
| 0.75 | 7.1 | 10.5 | 0.82 | 5.7 |
| 0.98 | 7.6 | 7.1 | 0.88 | 8.6 |
| 1.16 | 7.5 | 6.2 | 0.87 | 7.8 |
| 1.31 | 7.7 | 6.0 | 0.90 | 9.6 |

a) Values were determined from analysis of TGA curves acquired at 2 °C/min.

**Table 4.** Thermodynamic quantities obtained from thermal analysis experiments.

| monomer loss ratio, $\rho$ | $\Delta H$ amidization[a] [J/g] | $\Delta H$ imidization[a] [J/g] | $E_a$ amidization[b] [kJ/mol] | $E_a$ imidization[c] [kJ/mol] |
|---|---|---|---|---|
| 0.68 | -21.3 | 119 | 109 | 142 |
| 0.75 | -29.4 | 109 | 118 | 133 |
| 0.98 | -30.4 | 125 | 114 | 125 |
| 1.16 | -32.5 | 131 | 132 | 128 |
| 1.31 | -36.7 | 131 | 134 | 165 |

a) Determined from DSC scans at 40 ºC/min.
b) Determined using Kissinger method where $T_f$ corresponds to the peak of the DSC exotherm.
c) Determined using Kissinger method where $T_f$ corresponds to a 4% mass loss from TGA curves acquired at different heating rates.

**LIST OF FIGURES**

**Graphical Abstract**

# An Investigation of Solid-State Amidization and Imidization Reactions inVapor Deposited Poly(amic acid)

Mitchell Anthamatten[1]*, Stephan A. Letts[1], Katherine Day[1], Robert C. Cook[1], Anthony P. Gies[2], Tracy P. Hamilton[2], William K. Nonidez[2]

1) Lawrence Livermore National Laboratory, P.O. Box 808, M.S. L-474 Livermore, CA 94550 USA
2) Department of Chemistry, University of Alabama at Birmingham, 901 14th Street South, Birmingham, AL 35294 USA
* Current Address: University of Rochester, Department of Chemical Engineering, 206 Gavett Hall, Rochester, NY, 14627.

The condensation polymerization reaction of 4,4'-oxydianiline (ODA) with pyromellitic dianhydride (PMDA) to form poly(amic acid) and the subsequent imidization reaction to form polyimide were investigated for films prepared using vapor deposition polymerization techniques. Fourier-transform infrared spectroscopy (FT-IR), thermal analysis, and matrix-assisted laser desorption/ionization time-of-flight mass spectrometry (MALDI-TOF MS) of films at different temperatures indicate that additional solid-state polymerization occurs prior to imidization reactions. Experiments reveal that, upon vapor deposition, poly(amic acid) oligomers form that have a number-average molecular weight of about 1500 Daltons. Between 100 – 130 ºC these chains undergo additional condensation reaction to form slightly higher molecular weight oligomers. Calorimetry measurements show that this reaction is exothermic ($\Delta H \sim -30$ J/g) with an activation energy of about 120 kJ/mol. Experimental reaction enthalpies are compared to results from *ab initio* molecular modeling calculations to estimate the number of amide groups formed. At higher temperatures (150 – 300 °C) imidization of amide linkages occurs as an endothermic reaction ($\Delta H \sim +120$ J/g) with an activation energy of about 130 kJ/mol. Solid-state kinetics were found to depend on reaction conversion as well as the processing conditions used to deposit films.

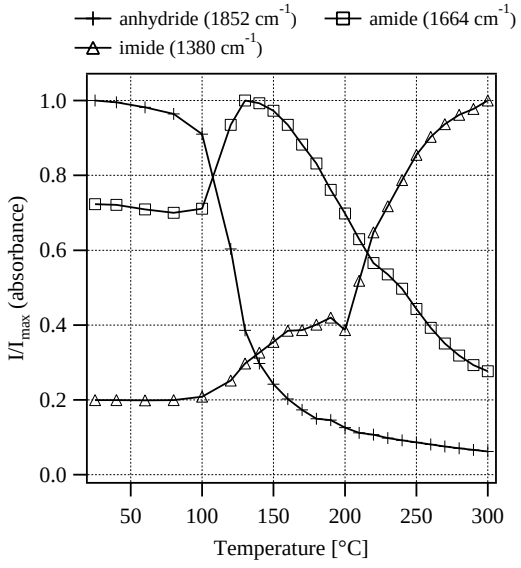

## References


1. Sroog, C. E. In Polyimides Fundamentals and Applications; Ghosh, M. K.; Mittal, K. L., Eds.; Marcel Dekker: New York, 1996, p 1-6.
2. Strunskus, T.; Grunze, M. In Polyimides Fundamentals and Applications; Ghosh, M. K.; Mittal, K. L., Eds.; Marcel Dekker: New York, 1996, p 187-205.
3. Salem, J. R.; Sequeda, F. O.; Duran, J.; Lee, W. Y.; Yang, R. M. Journal of Vacuum Science and Technology 1986, 4, 369-374.
4. Iijima, M.; Takahashi, Y.; Inagawa, K.; Itoh, A. J. Vac. Sci. Jpn. 1985, 28, 437-439.
5. Koros, W. J.; Story, B. J.; Jordan, S. M.; O'Brien, K. C.; Husk, G. R. Polymer Engineering and Science 1987, 27, 603-610.
6. O'Brien, K. C.; Koros, W. J.; Husk, G. R. Journal of Membrane Science 1988, 35, 217-230.
7. Yanagishita, H.; Kitamoto, D.; Haraya, K.; Nakane, T.; Okada, T.; Matsuda, H.; Idemoto, Y.; Koura, N. Journal of Membrane Science 2001, 188, 165-172.
8. Malba, V.; Liberman, V.; Bernhardt, A. F. J. Vac. Sci. Technol. A. 1997, 15, 844-849.
9. Liberman, V.; Malba, V.; Bernhardt, A. F. IEEE Trans. on Components, Packaging, and Manufact. Tech- Part B 1997, 20, 13-16.
10. Lee, B.-J.; Kim, H.-G.; Kim, Y.-B.; Park, K.-H.; Lee, D.-C. Polymer (Korea) 1997, 21, 682-688.
11. Sanchez, J. J.; Letts, S. A. Fusion Technology 1997, 31, 491-496.
12. Alfonso, E. L.; Chen, S. H.; Gram, R. Q.; Harding, D. R. J. Mater. Res. 1998, 13, 2988-3000.
13. Roberts, C. C.; Orthion, P. J.; Hassel, A. E.; Parrish, B. K.; Buckley, S. R.; Fearon, E.; Letts, S. A.; Cook, R. C. Fusion Technology 2000, 38, 94-107.
14. Tsai, F.-Y.; Alfonso, E. L.; Harding, D. R.; Chen, S. H. J. Phys. D: Appl. Phys. 2001, 34, 3011-3018.
15. Letts, S. A.; Nissen, A. E.; Orthion, P. J.; Buckley, S. R.; Fearon, E.; Chancellor, C.; Roberts, C. C.; Parrish, B. K.; Cook, R. C. Fusion Technology 2002, 41, 268-277.
16. Letts, S.; Anthamatten, M.; Buckley, S.; Fearon, E.; Nissen, A. E.; Cook, R. Fusion Technology 2004, 45, 180-186.
17. Nicholson, L. M.; Whitley, K. S.; Gates, T. S.; Hinkley, J. A. Journal of Materials Science 2000, 35, 6111-6121.
18. Chang, J. H.; Kwang, M. P. European Polymer Journal 2000, 36, 2185-2191.
19. Tsai, F. Y.; Alfonso, E. L.; Chen, S. H.; Harding, D. R. Fusion Technology 2000, 38, 83-89.
20. Jou, J.; Cheng, C.; Jou, E. C.; Yang, A. C. Journal of Polymer Science: Part B: Polymer Physics 1996, 34, 2239-2246.
21. Ito, Y.; Hikita, M.; Kimura, T.; Mizutani, T. Japanese Journal of Applied Physics 1990, 29, 1128-1131.
22. Takahashi, Y.; Iijima, M.; Inagawa, K.; Itoh, A. J. Vac. Sci. Technol. A. 1987, 5, 2253-2256.
23. Dimitrakopoulos, C. D.; Machlin, E. S.; Kowalczk, S. P. Macromolecules 1996, 29, 5818-5825.

24. Cotts, P. M.; Volksen, W.; Ferline, S. Jounal of Polymer Science: Part B: Polymer Physics 1992, 30, 373-379.
25. Wallach, M. L. Journal of Polymer Science: Part A-2 1967, 5, 653-662.
26. Volksen, W.; Cotts, P. M.; Yoon, D. Y. Journal of Polymer Science: Part B: Polymer Physics 1987, 25, 2487-2495.
27. Kim, S.; Cotts, P. M.; Volksen, W. Journal of Polymer Science: Part B: Polymer Physics 1992, 30, 177-183.
28. Gies, A. P.; Nonidez, W. K.; Anthamatten, M.; Cook, R. C.; Mays, J. W. Rapid Commun. Mass Spectrom. 2002, 16, 1-8.
29. Roberts, C. C.; Letts, S. A.; Saculla, M. D.; Hsieh, E. J.; Cook, R. C. Fusion Technology 1999, 35, 138-146.
30. Gies, A. P.; Nonidez, W. K. Anal. Chem. 2004, 2004, 1991-1997.
31. IGOR Pro v4.0 was used for non-linear regression.
32. Hsu, T. C. J.; Liu, Z. L. Journal of Applied Polymer Science 1992, 46, 1821-1833.
33. Navarre, M. In Polyimides: Synthesis, Characterization, and Applications; Mittal, K. L., Ed.; Plenum Press: New York, 1984, p 429-442.
34. Kissinger, H. E. Anal. Chem. 1957, 29, 1702.
35. Kissinger, H. E. J. Res. Nat. Bur. Stand. 1956, 57, 217.
36. Starink, M. J. Thermochimica Acta 2003, 404, 163-176.
37. Gies, A. P.; Nonidez, W. K.; Anthamatten, M.; Cook, R. C. Macromolecules, In Press 2004.
38. Kong, J.; White, C. A.; Krylov, A. I.; Sherrill, C. D.; Adamson, R. D.; Furlani, T. R.; Lee, M. S.; Lee, A. M.; Gwaltney, S. R.; Adams, T. R.; Ochsenfeld, C.; Gilbert, A. T. B.; Kedziora, G. S.; Rassolov, V. A.; Maurice, D. R.; Nair, N.; Shao, Y.; Besley, N. A.; Maslen, P. E.; Dombroski, J. P.; Dachsel, H.; Zhang, W. M.; Korambath, P. P.; Baker, J.; Byrd, E. F. C.; Van Voorhis, T.; Oumi, M.; Hirata, S.; Hsu, C. P.; Ishikawa, N.; Florian, J.; Warshel, A.; Johnson, B. G.; Gill, P. M. W.; Head-Gordon, M.; Pople, J. A. J. Computational Chemistry 2000, 21, 1532.
39. Frisch, M. J.; Trucks, G. W.; Schlegel, H. B.; Scuseria, G. E.; Robb, M. A.; Cheeseman, J. R.; Zakrzewski, V. G.; Montgomery, J., J. A.; Stratmann, R. E.; Burant, J. C.; Dapprich, S.; Millam, J. M.; Daniels, A. D.; Kudin, K. N.; Strain, M. C.; Farkas, O.; Tomasi, J.; Barone, V.; Cossi, M.; Cammi, R.; Mennucci, B.; Pomelli, C.; Adamo, C.; Clifford, S.; Ochterski, J.; Petersson, G. A.; Ayala, P. Y.; Cui, Q.; K. Morokuma; Makick, D. K.; Rabuck, A. D.; Raghavachari, K.; Foresman, J. B.; Cioslowski, J.; Ortiz, J. V.; Baboul, A. G.; Stefanov, B. B.; Liu, G.; Lianshenko, A.; Piskorz, P.; Komaromi, I.; Gomperts, R.; Martin, R. L.; Fox, D. J.; Keith, T.; Al-Laham, M. A.; Peng, C. Y.; Nanayakkara, A.; Gonzalez, C.; Challacombe, M.; Gill, P. M. W.; Johnson, B.; Chen, W.; Wong, M. W.; Andres, J. L.; Gonzalez, C.; Head-Gordon, M.; Replogle, E. S.; Pople, J. A. In Gaussian 98: Pittsburg, PA, 1998.

**Figure 1**

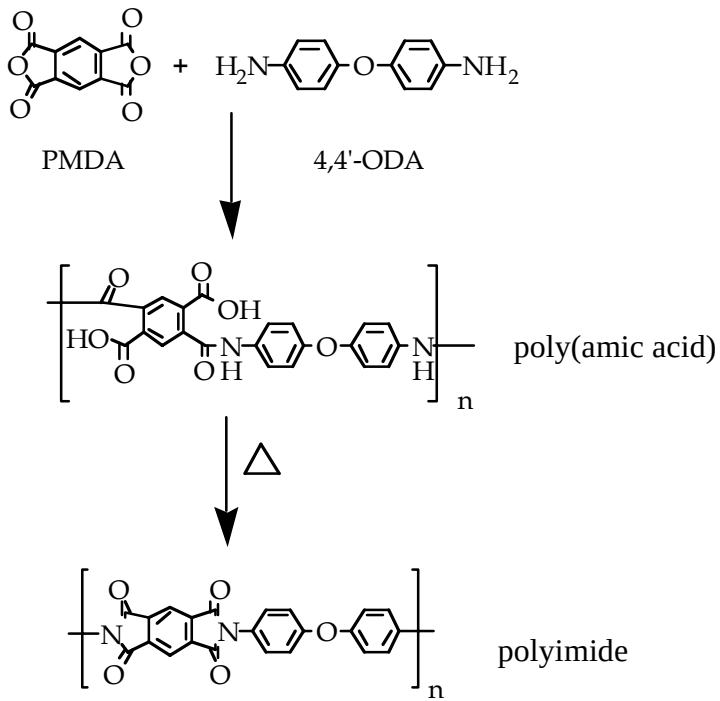

**Figure 2**

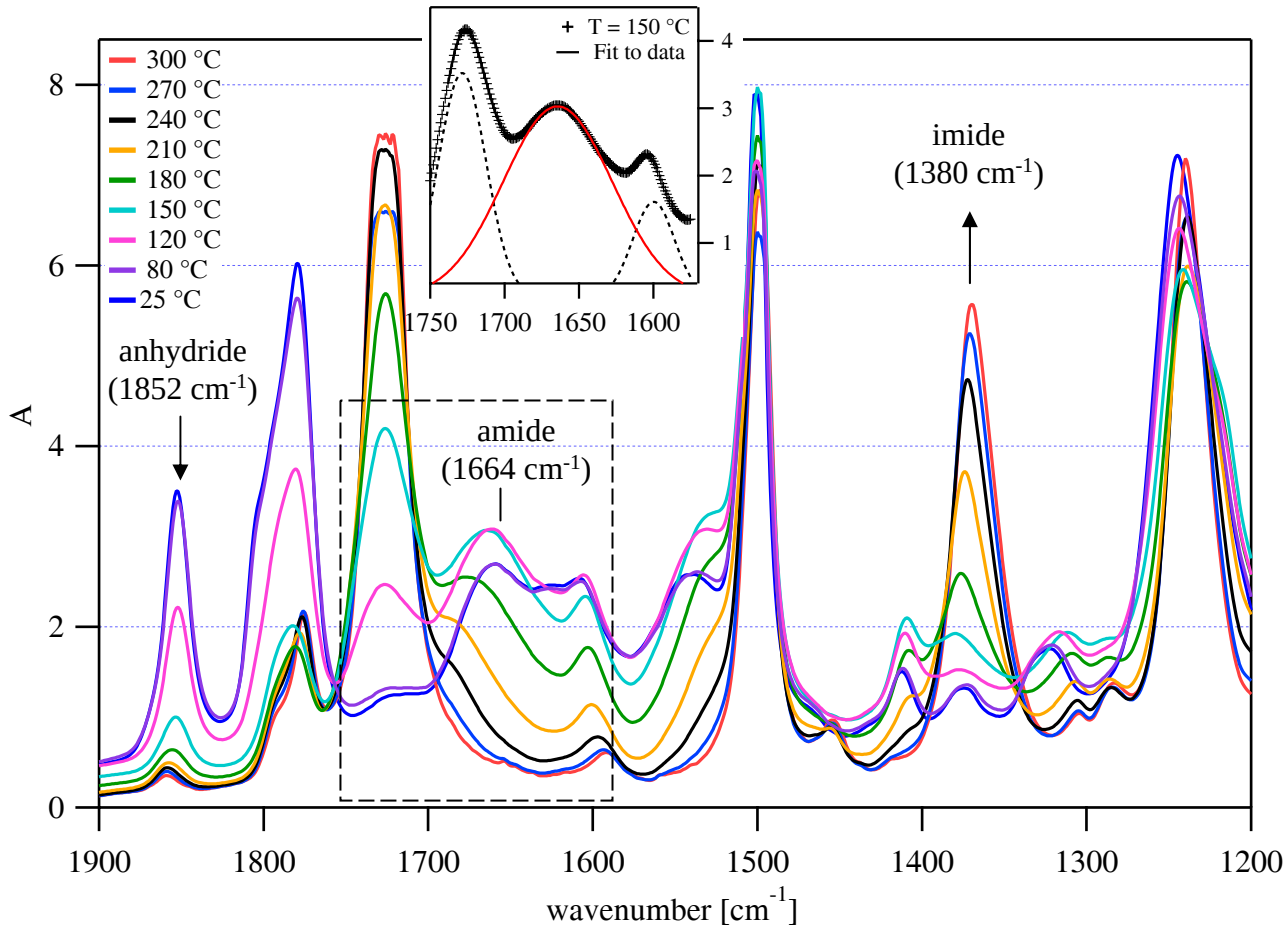
300 °C
270 °C
240 °C
210 °C
180 °C
150 °C
120 °C
80 °C
25 °C
anhydride
(1852 cm-1)
amide
(1664 cm-1)
imide
(1380 cm-1)
T = 150 °C
Fit to data
A
wavenumber [cm-1]
0
2
4
6
8
1900
1800
1700
1600
1500
1400
1300
1200
1750
1700
1650
1600
1
2
3
4

**Figure 3**

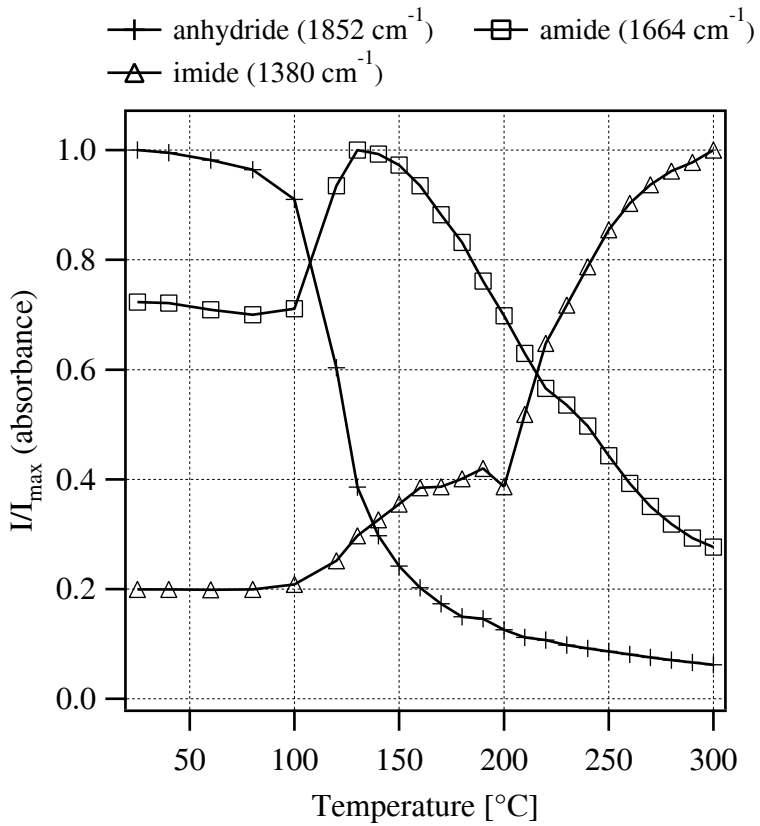
anhydride (1852 cm-1)
amide (1664 cm-1)
imide (1380 cm-1)
1.0
0.8
0.6
0.4
0.2
0.0
I/Imax (absorbance)
50
100
150
200
250
300
Temperature [°C]

**Figure 4**

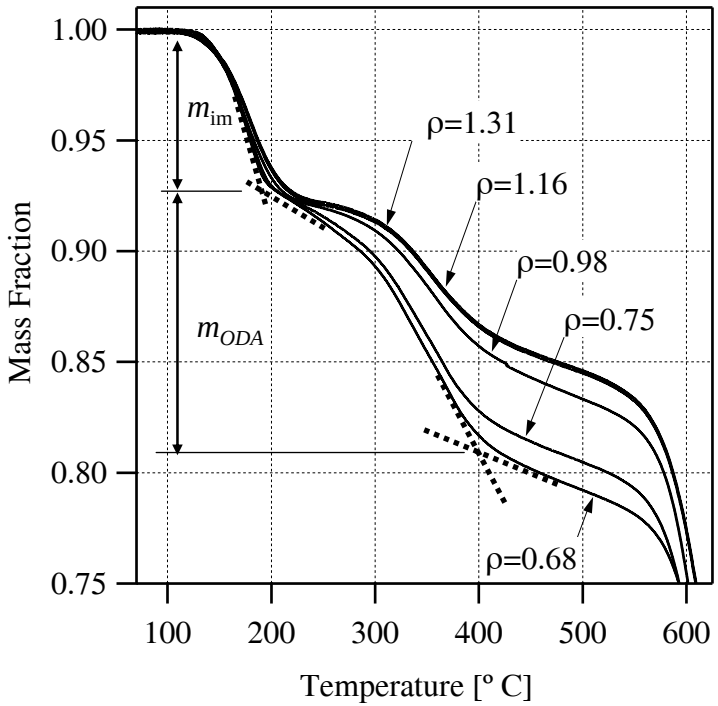
1.00
0.95
0.90
0.85
0.80
0.75
Mass Fraction
100
200
300
400
500
600
Temperature [° C]
$m_{im}$
$m_{ODA}$
ρ=1.31
ρ=1.16
ρ=0.98
ρ=0.75
ρ=0.68

**Figure 5**

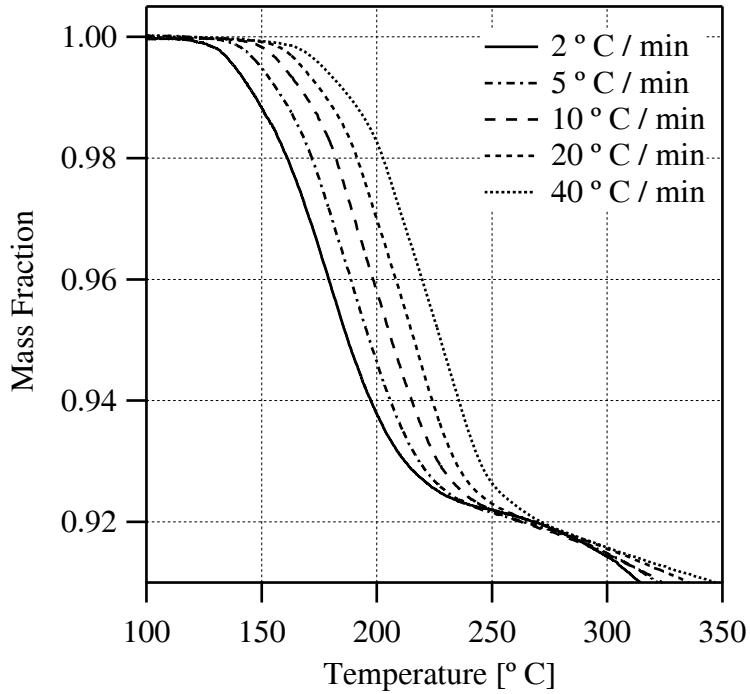
1.00
0.98
0.96
0.94
0.92
Mass Fraction
100
150
200
250
300
350
Temperature [° C]
2 ° C / min
5 ° C / min
10 ° C / min
20 ° C / min
40 ° C / min

**Figure 6**

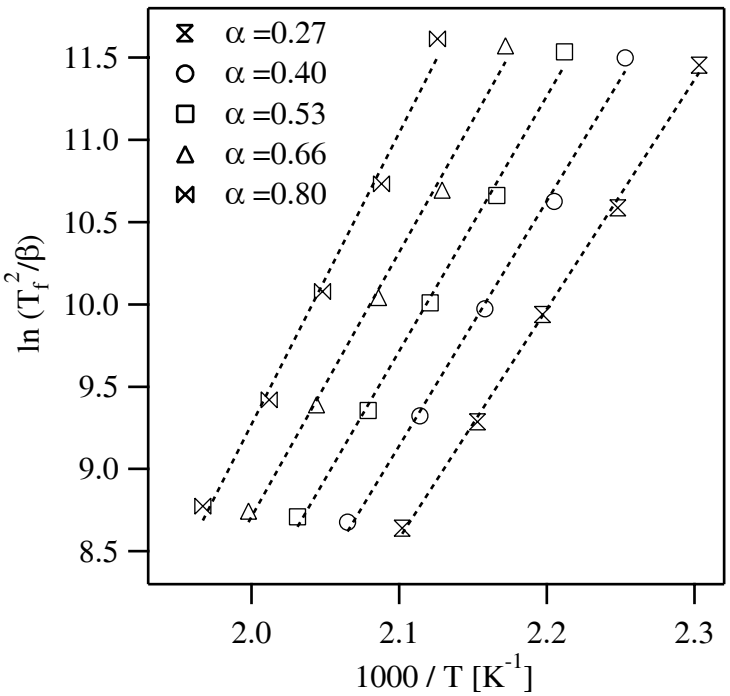
α =0.27
α =0.40
α =0.53
α =0.66
α =0.80
11.5
11.0
10.5
10.0
9.5
9.0
8.5
ln (T_f^2/β)
2.0
2.1
2.2
2.3
1000 / T [K^-1]

**Figure 7**

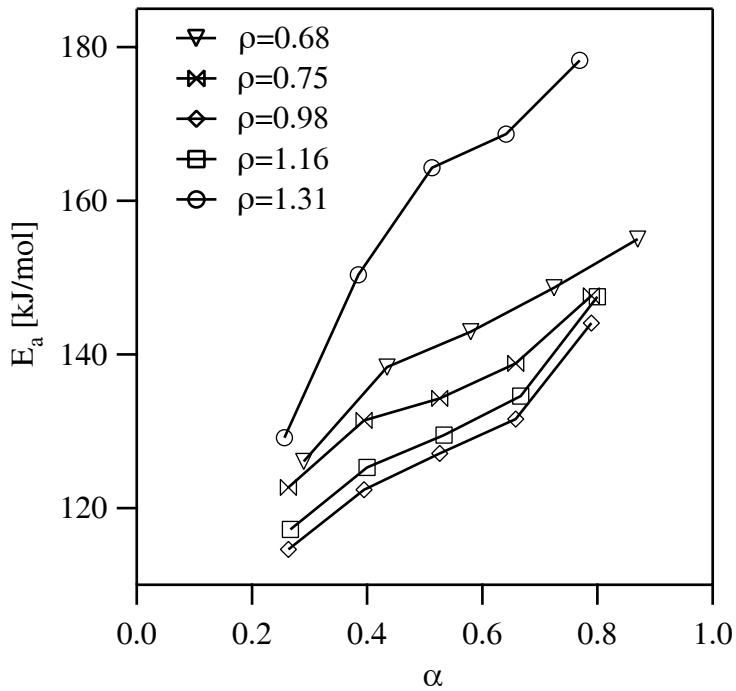
ρ=0.68
ρ=0.75
ρ=0.98
ρ=1.16
ρ=1.31
180
160
140
120
E_a [kJ/mol]
0.0
0.2
0.4
0.6
0.8
1.0
α

**Figure 8**

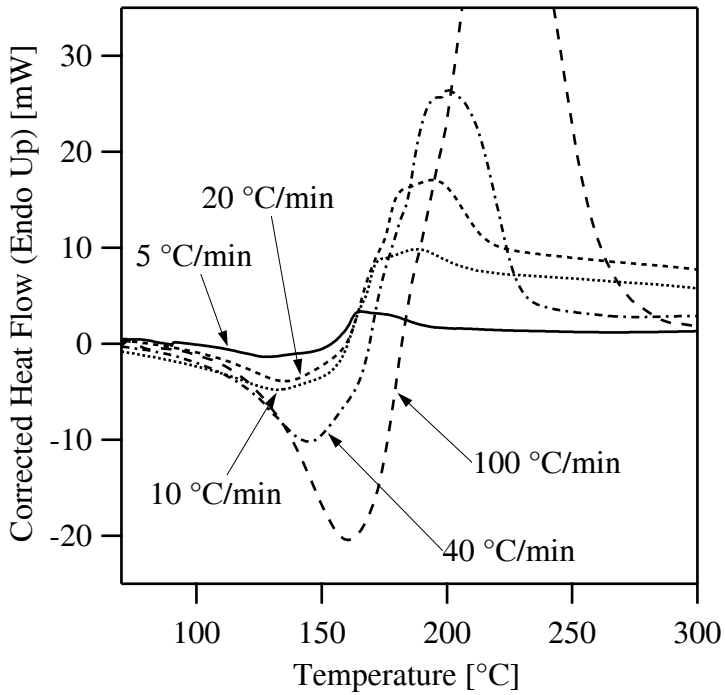
Corrected Heat Flow (Endo Up) [mW]
30
20
10
0
-10
-20
100
150
200
250
300
Temperature [°C]
20 °C/min
5 °C/min
10 °C/min
100 °C/min
40 °C/min

**Figure 9**

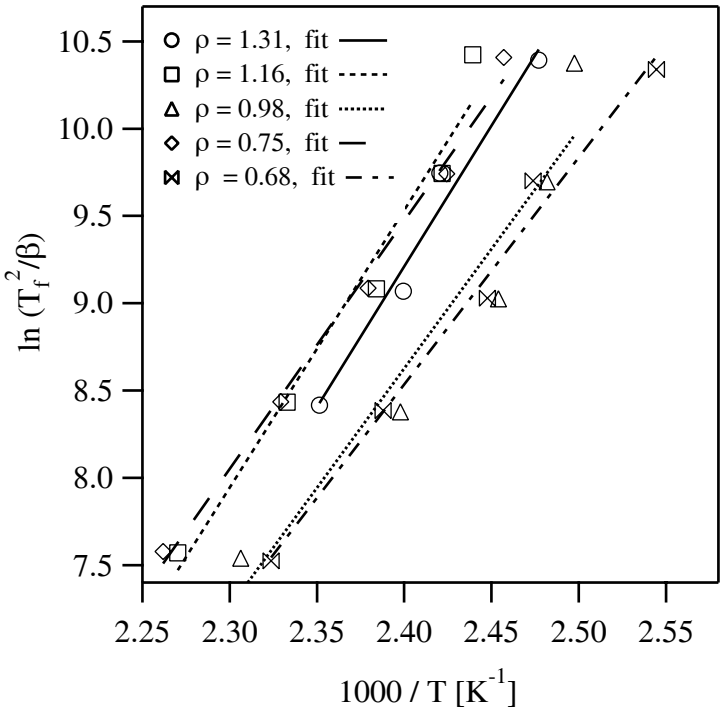
ρ = 1.31, fit
ρ = 1.16, fit
ρ = 0.98, fit
ρ = 0.75, fit
ρ = 0.68, fit
10.5
10.0
9.5
9.0
8.5
8.0
7.5
ln (T_f^2/β)
2.25
2.30
2.35
2.40
2.45
2.50
2.55
1000 / T [K^-1]

# Figure 10

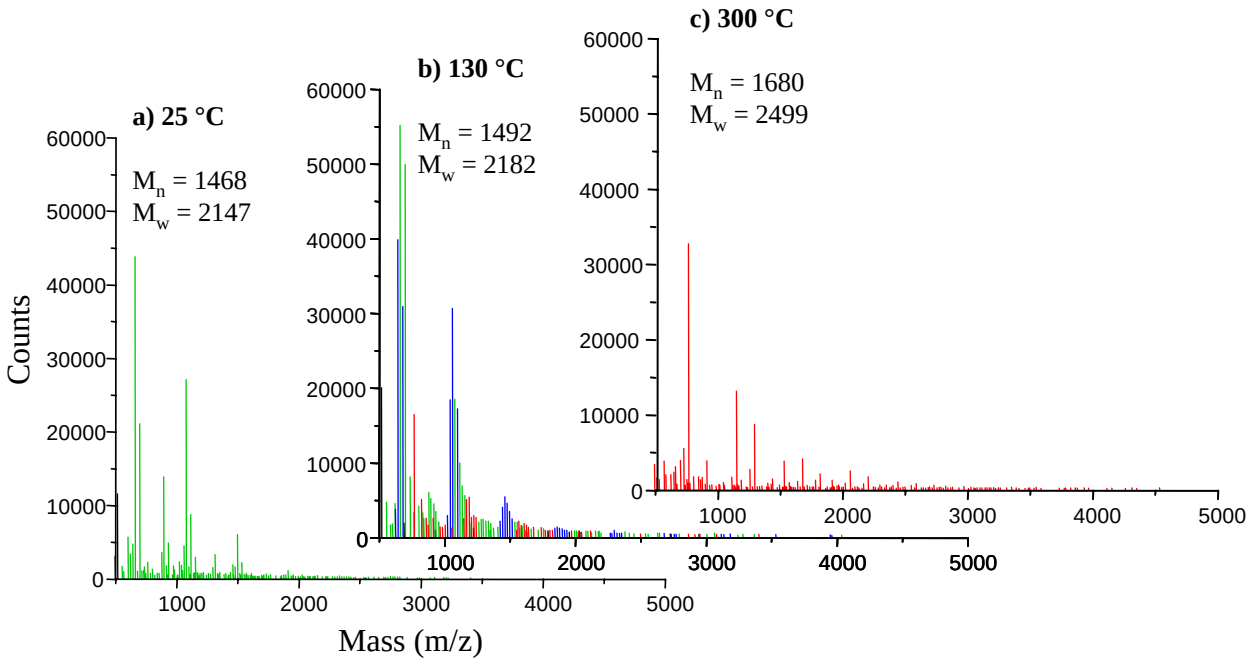
a) 25 °C
$M_n$ = 1468
$M_w$ = 2147
b) 130 °C
$M_n$ = 1492
$M_w$ = 2182
c) 300 °C
$M_n$ = 1680
$M_w$ = 2499
Counts
Mass (m/z)
0
10000
20000
30000
40000
50000
60000
1000
2000
3000
4000
5000